Available online at www.sciencedirect.com

ScienceDirect

Procedia Engineering 160 (2016) 214 – 222

Procedia Engineering

www.elsevier.com/locate/procedia

XVIII International Colloquium on Mechanical Fatigue of Metals (ICMFM XVIII)

Effect of weld defects on the fatigue strength of ultra high-strength steels

M. J. Ottersböck[a]*, M. Leitner[a], M. Stoschka[a], W. Maurer[b]

[a]*Montanuniversität Leoben, Franz-Josef-Straße 18, 8700 Leoben, Austria*
[b]*voestalpine Stahl GmbH, voestalpine-Straße 3, 4020 Linz, Austria*

Abstract

Enhancing the lightweight potential of mobile steel structures by applying high-strength steels and reducing sheet thicknesses leads to a significant increase of energy effectiveness and a reduction of noxious emissions during operation. However, due to this increase of yield and tensile strength, fracture toughness decreases and notch sensitivity rises. Hence, the local weld geometry becomes more important, especially in case of ultra high-strength steels. This paper deals with the detection and assessment of common geometric weld defects, such as undercuts, and their effect on the fatigue strength of ultra high-strength steel joints. For this purpose, butt joint specimens are welded incorporating ultra high-strength steel as base material. All specimens are judged by visual testing and the detected weld defects undergo an additional surface topography measurement prior to fatigue testing. First, an image processing based *Matlab*©-Routine is built up to evaluate the local geometrical properties of the weld toe including undercuts. Second, a numerical model of the actual weld geometry is generated. This is utilized to perform numerical analyses in order to compute the actual stress concentration factors as well as fatigue parameters in terms of notch stresses. The experimental work covers fatigue tests of undercut-imperfected and defect-free specimens in order to contribute to the effect of such defects on fatigue life. Finally, an enhanced fatigue assessment of welds with undercuts and high-quality joints is performed based on numerical investigations and validated by experimental results.

Peer-review under responsibility of the University of Oviedo

Keywords: Fatigue; ultra high-strength steel; welding; weld defects; weld topography

* Corresponding author. Tel.: +43-3842-402-1472; fax: +43-3842-402-1402.
E-mail address: markus.ottersboeck@unileoben.ac.at

Peer-review under responsibility of the University of Oviedo
doi:10.1016/j.proeng.2016.08.883

1. Introduction

The today's trend of environmental friendly construction and operation of mobile crane, heavy freight or special purpose vehicles leads to increased requirements regarding to lightweight design. The application of high-strength or ultra high-strength steels enables a reduction of sheet thickness and is therefore used to reduce vehicle weight in prevailing static load cases. But for cyclic service loading, current fatigue design guidelines for welded structures such as [1] and [2] do not consider the effect of base material yield strength. It is conservatively reasoned that even good workmanship manufactured weld seams possess initial cracks. Besides, it is assumed that all construction steels exhibit a similar crack propagation behavior. Thus, the crack initiation phase is neglected resulting in a fatigue behavior of welded joints independent of the base material steel grade. On the other hand, recent publications tend towards increasing weld fatigue strength utilizing high-strength base materials [3, 4]. Basically, one condition for the applicability of the higher yield strength is the prolongation of the crack initiation phase. This can be ensured by manufacturing high quality welds assuring a smooth weld transition and the exclusion of any severe notches such as undercuts, pores or lack of fusion. One measure to meet these conditions is the optimization of the welding parameters maintaining a smooth and uniform weld topology [5]. Post-weld-treatment methods such as TIG-dressing [6] or HFMI-treatment [7] are further process options to affect the weld toe region beneficially.

This work investigates the effect of single undercuts as characteristic weld defects on the fatigue behavior of high quality ultra high-strength steel welds. A *6 mm* ultra high-strength steel *S1100* is used as base material for this investigation. The sheets are butt-welded in two passes using *G89MC* wire as filler metal. In order to produce small individual undercuts, the welding process parameters knowingly deviate from the optimum process settings. Subsequently, the sheets are cut to specimen shape; the weld root is ground flush to plate to focus on the topology of the weld toe. After removal of process slag from the weld toe, all specimens are visually examined for any weld defects on the surface. Ten of them exhibit undercuts in different shapes and sizes even visible to the naked eye, one is depicted in Fig. 1a. The defect-free specimens were fatigue tested immediately, whereas the defective ones undergo further investigations of the weld surface topography.

2. Weld topography

The local weld geometry is important regarding to the fatigue behavior of welded joints [8 - 10]. In particular, the undercuts shape has a significant influence on the crack initiation phase [11, 12]. Therefore, the weld toe topology of the ten undercut-defective specimens is measured in detail. For this purpose an optical 3D surface measurement device *Alicona InfiniteFocus*® utilizing the focus-variations measurement principle is used. Both weld toes of the butt joint are scanned using the same global coordinate system with a *2.5x* objective magnification. This keeps the resulting data on a manageable size level and allows a minimum measureable radius of $20\ \mu m$ and a corresponding maximum slope angle of $87°$ [13].

2.1. Data processing

The data in form of the spatial xyz-coordinates is subsequently processed and analysed by a user-defined *Matlab*®-routine. The first steps within this procedure are the exclusion of outlying data points and the connection of the two separate scans for both weld toes using spatial interpolation of the weld reinforcement. Finally the number of data points is reduced by a surface fitting algorithm for further analysis. A sample result for the weld in Fig. 1a is shown in Fig. 1b.

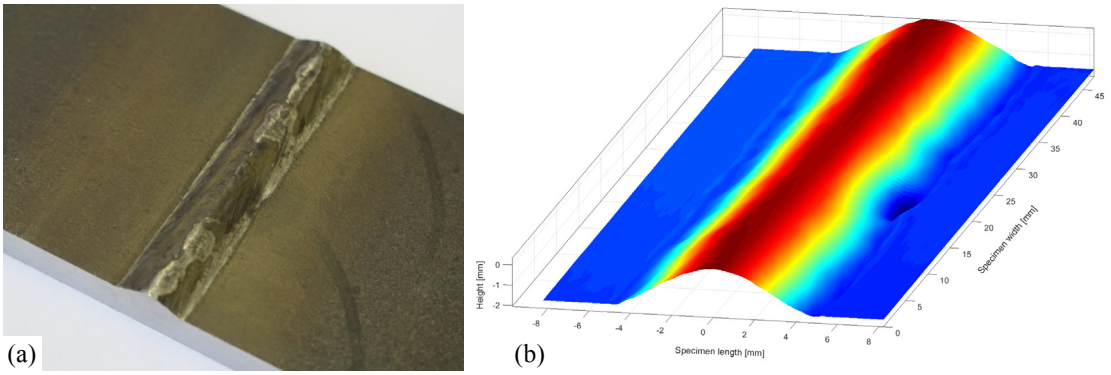

Fig. 1. (a) Specimen geometry with weld toe exhibiting an undercut; (b) Result of the surface measurement and data processing

The main task of the data analysis covers the calculation of undercut depth and weld reinforcement angle over the specimen width. Therefore, the *Matlab*® implemented Hough transformation algorithm [14] is applied, a feature extraction technique to find imperfect instances of parameterized geometric shapes used in digital image processing. The resulting spatial geometry is sliced into *120* sections where each weld toe image is processed separately. As the digital image processing method operates with binary pictures, the course of each weld topology is converted to a white pixel-line with black background at first. Subsequently, the Hough transformation algorithm is applied twice using different boundary conditions to determine the sheet level and the course of the weld reinforcement. It is possible, that this algorithm leads to more than one straight line. In this case, the results are weighted by their adjacent line length and averaged to obtain the final result shown in Fig. 2. The undercut depth is then calculated by the orthogonal distance from the local minimum to the sheet level. The weld reinforcement angle is the result of the difference between the sheet level and the weld reinforcement line.

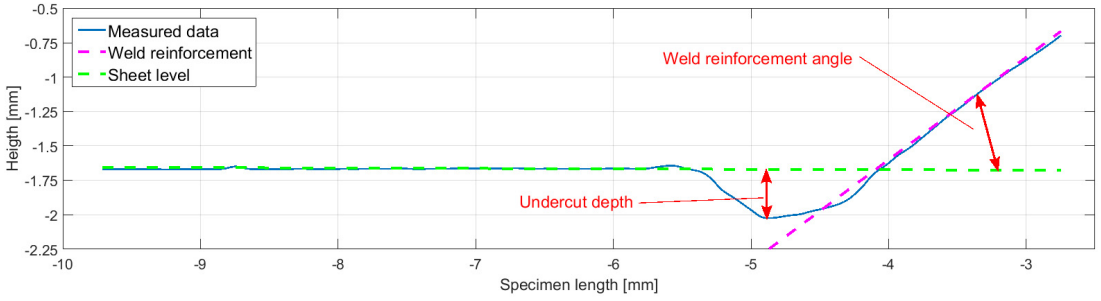

Fig. 2. Result of the Hough transformation with the definition of undercut depth and weld reinforcement angle

Finally, the specimen geometry including the weld topography is converted to NURBS-surfaces. Thus, the geometry is suitable for the export to the finite element software *Abaqus*®, which is applied for further numerical analysis. The main advantage of NURBS-surfaces is the capability to transfer a mathematical defined geometry. This allows maximum flexibility in regard to the meshing of the part for finite element analysis without any reduction in accuracy.

2.2. Surface measurement results

The surface measurement data processing is automatically performed for each of the ten specimens exhibiting at least one visible undercut. The results of each section are put together leading to a course of the weld reinforcement angle and undercut depth over specimen width. Fig. 3 summarizes this outcome exemplarily for the welded specimen shown in Fig. 1. Both, the course of weld reinforcement angle and undercut depth clearly prove the

presence of an undercut-defect. Whereas the average reinforcement angle is at about *25* to *30°*, the undercut exhibits a significantly steeper angle of nearly *40°*. Similarly, the average undercut value is below *0.05 mm* and the maximum shows a depth of about *0.4 mm*. This behaviour is observed within all ten specimens leading to the conclusion that this method is suitable for the detection of undercuts, if weld slag is removed prior to the measurements.

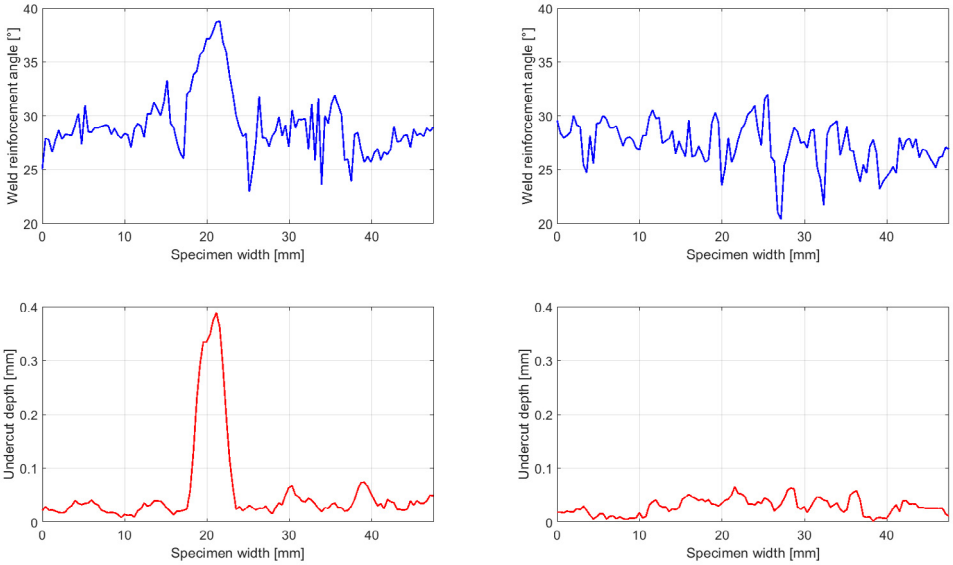

Fig. 3. Surface measurement results exemplarily for one specimen

3. Fatigue tests

Load-controlled constant amplitude fatigue tests are carried out at a tumescent tensile stress ratio of *R=0.1* up to burst fracture. The tests are mainly performed at a *1 MN* servo hydraulic test rig at a test frequency of *10 Hz*. Only non-defective specimens in high-cycle fatigue domain are tested on a resonance pulsator at frequencies of around *70 Hz* to shorten the test times. The statistical evaluation of the results in finite life regime is performed according to [15] with arbitrary slope values whereas the high cycle fatigue region is estimated using the approach presented in [16] with a decrease of *10%* per decade in fatigue strength corresponding to a slope of *k=22,* as suggested in [17].

Fig. 7a depicts the fatigue test results as SN-curve. The coloured graph shows the evaluation of the defective specimen in red, the non-defective in green and the overall evaluation in blue dye. It can be clearly seen, that defects do have a negative influence on the fatigue strength. Surprisingly, the negative effect decreases somewhat with the load level leading to similar fatigue test results in the high-cycle fatigue region. This can be reasoned by varying residual stress states especially in the surface layer. Another explanation could be that visually defect-free specimen even exhibit very small defects at the weld toe. In this context, Fig. 4 shows the fracture surfaces of one undercut-defective and one defect-free specimen. Both are tested at $\Delta\sigma$*=200 MPa* and failed at very similar load cycle numbers. The undercut of the visually defective specimen in Fig. 4b is clearly visible compared to the specimen without undercut defect in Fig. 4a. In this picture a small indentation, marked by a red arrow, is visible in the area of the crack initiation point which would support the abovementioned theory.

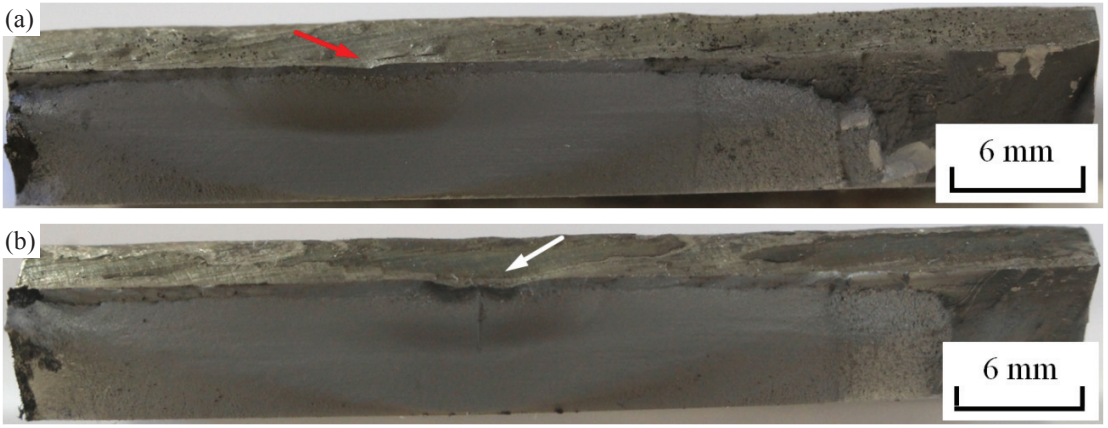

Fig. 4. Fracture surfaces: (a) *Δσ=200 MPa*, *N~3e6*; (b) *Δσ=200 MPa*, *N~2.87e6* with clearly visible undercut (Specimen of Fig. 1)

4. Fatigue assessment

This chapter focuses on linking the fatigue test results of the undercut-defective and non-defective specimen by a local support effect qualifier to ensure comparability for these high-strength steel joints.

4.1. Numerical stress analysis

The numerical investigations using *Abaqus*© FEA-software cover the determination of the stress concentration factors of the undercut-defective specimen using their actual geometry from surface measurements as described in chapter 2. Based on the NURBS-surface of the weld topography, a three-dimensional model is built up with a sheet thickness of *6 mm*. Thus, all geometric misalignments are included in the simulation as they are part of the surface measurement. The model is meshed using quadratic hexahedral elements with reduced integration *(C3D20R)*. The mesh density is adapted to the geometry with very fine mesh at the surface of the weld toe where the highest stress gradients are assumed. In numbers, this means an edge length of approximately *0.03 mm* across the weld toe and *0.25 mm* in direction of the specimen width. Subsequently, linear elastic simulations with a unit load are carried out for each model. Fig. 5 shows the local mesh distribution at the weld and the stress distribution over the weld and an undercut.

An interesting outcome of the results of the numerical simulations and the fracture surface analysis is the comparison of the point with the highest linear elastic stress in simulation and the actual crack initiation point at the real specimen. In eight of ten cases these points are identical. In the other two cases the specimen exhibits at least two adjacent notches, where the crack initiated from the second highest stress concentration.

4.2. Support effect of ultra high-strength steel

The local support effect of *S1100* base material was part of previous investigations examined in [18], see Fig. 6a. A mathematical model based on [19] is set up to describe the notch support factor n_σ by the local relative stress gradient χ^* with a material dependent exponent K_D (Equation (1)). The parameters of this formula were evaluated at three load cycle numbers: *1e5*, *1e6* and *1e7* representing the chosen run-out level; the obtained result is presented in Table 1. Fig. 6b shows the course of n_σ over χ^* according to Equation (1) and the experimental data fits quite well to the supporting effect relationship based on local relative stress gradient.

$$\frac{K_t}{K_f} = n_\sigma\left(\chi^*\right) = 1 + \left(\left(\frac{\Delta\sigma_{notched}}{\Delta\sigma_{unnotched}}\right) - 1\right) \cdot \left(\frac{\chi^*}{\chi^*_{notched}}\right)^{K_D} \tag{1}$$

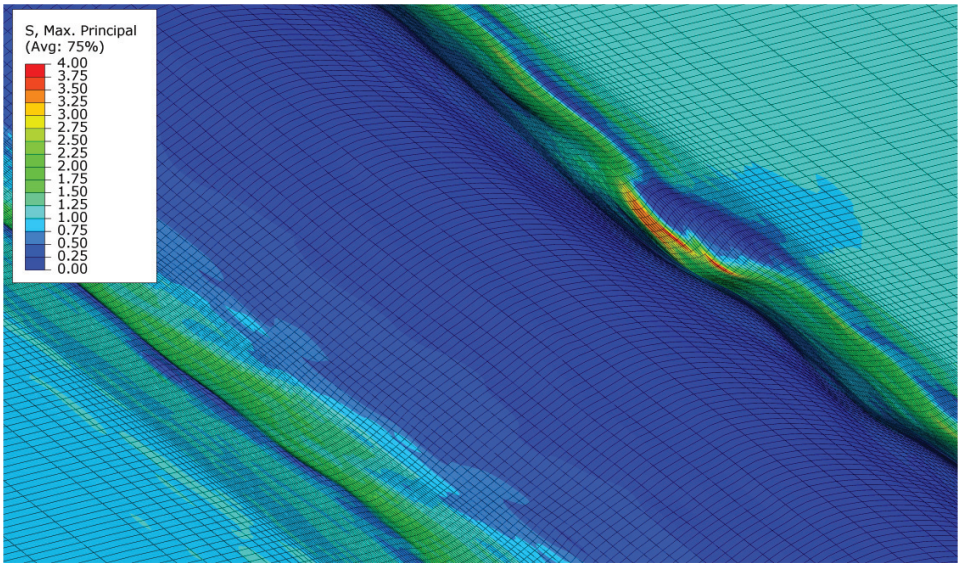

Fig. 5. Local mesh at the weld with stress distribution around an undercut

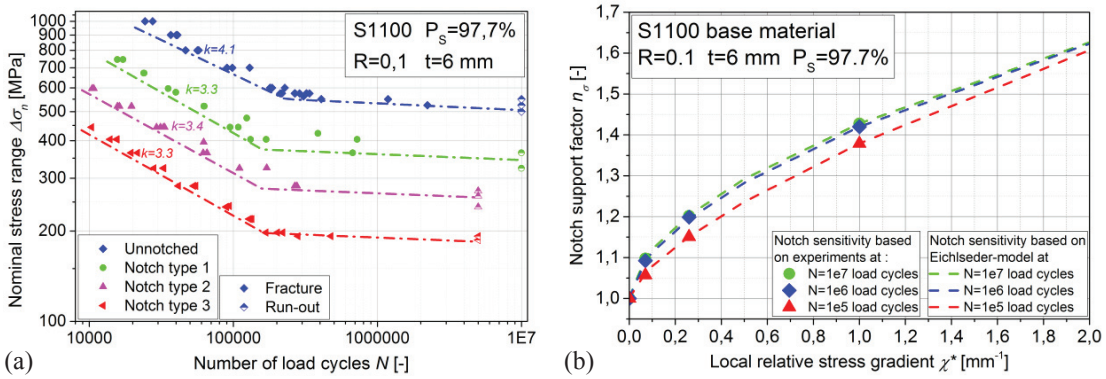

Fig. 6. (a) SN-curve of unnotched and notched base material specimen; (b) Notch support effect of S1100 base material

Table 1. Parameters for mathematical description of support effect for S1100 base material

Numbers of load cycles N	1e5	1e6	1e7
$\Delta\sigma_{unnotched}$ [MPa]	665	534	506
$\Delta\sigma_{notched}$ [MPa]	917	758	723
$\chi^*_{notched}$ [mm^{-1}]	1	1	1
K_D [-]	0.65	0.57	0.55

4.3. Recalculation of fatigue test results of defective specimen

As the undercut-defective specimens exhibit sharper notches than the defect-free, they benefit from higher support effect of the material thereby reducing the sharpness of the geometric notch. In order to compare the results,

the defective specimens are recalculated on the basis of the support effect of the base material. Therefore the definition of the fatigue notch factor K_f is set up for the defect-free welded specimen (index "Weld", Equation (2)) and the defective (index "Defective", Equation (3)). As the fatigue strength of the unnotched specimen is unknown, it is eliminated by equating (2) and (3) resulting in Equation (4). Thus, the fictive $\Delta\sigma_{Weld}$ of an undercut-defective specimen for a specific number of load cycles N can be calculated with the knowledge of stress concentration and notch support effect of both undercut-defective and defect-free specimen. Whereas the stress concentration is a direct output of the finite element simulation, the notch support results from the supporting effect model set up using the evaluated local relative stress gradient calculated from the simulation results. The required parameters of the support effect model are calculated by interpolation of the values in Table 1. The stress concentration factor and relative stress gradient for the defect-free weld are gained from simulation, where several weld toes without defects are evaluated and averaged. The calculations are performed using the actual crack initiation point instead of the highest stress concentration. The results are given in Table 2 in comparison with the respective experimental results. Specimen number 5 is excluded from further evaluations regarding fatigue strength, as crack initiation occurred under a weld spatter at the weld toe.

$$K_{fWeld}(N) = \frac{K_{tWeld}}{n_{\sigma Weld}(N)} = \frac{\Delta\sigma_{Weld}(N)}{\Delta\sigma_{unnotched}(N)} \tag{2}$$

$$K_{fDefective}(N) = \frac{K_{tDefective}}{n_{\sigma Defective}(N)} = \frac{\Delta\sigma_{Defective}(N)}{\Delta\sigma_{unnotched}(N)} \tag{3}$$

$$\Delta\sigma_{Weld}(N) = \Delta\sigma_{Defective}(N) \cdot \frac{K_{tWeld}}{K_{tDefecitve}} \cdot \frac{n_{\sigma Defective}(N)}{n_{\sigma Weld}(N)} \tag{4}$$

Table 2. Overview of the recalculation results for the defective specimen

	Numerical and analytical analysis			Experiment	
	K_t [-]	χ^* [mm^{-1}]	$\Delta\sigma_{Weld}$ [MPa]	$\Delta\sigma$ [MPa]	N [-]
Defect-free weld	3	7			
Defective specimen 1	3.93	10.327	674.8	600	23 497
Defective specimen 2	3.37	8.582	416.2	400	199 292
Defective specimen 3	3.975	9.872	236.5	200	2 281 981
Defective specimen 4	5.61	16.592	522.6	400	85 039
Defective specimen 5	6.178	16.308	306.7	200	2 873 617
Defective specimen 6	3.395	12.232	278.0	300	728 340
Defective specimen 7	3.915	14.287	204.5	200	3 958 013
Defective specimen 8	3.327	8.674	612.9	600	37 839
Defective specimen 9	3.801	9.953	661.1	600	25 060
Defective specimen 10	4.598	12.050	372.7	300	232 717

The outcome of the recalculations is displayed in Fig. 7b. In most cases the nominal stress range of the defective specimen is increased notably. With this correction, the local fatigue strength of the defective specimen is comparable to the non-defective specimen. Further on, the scatter index of the defective specimen is significantly reduced. This concludes that, based on an SN-curve obtained from non-defective specimen and their actual weld geometry, the effect of local undercuts or similar defects regarding to the fatigue strength can be estimated.

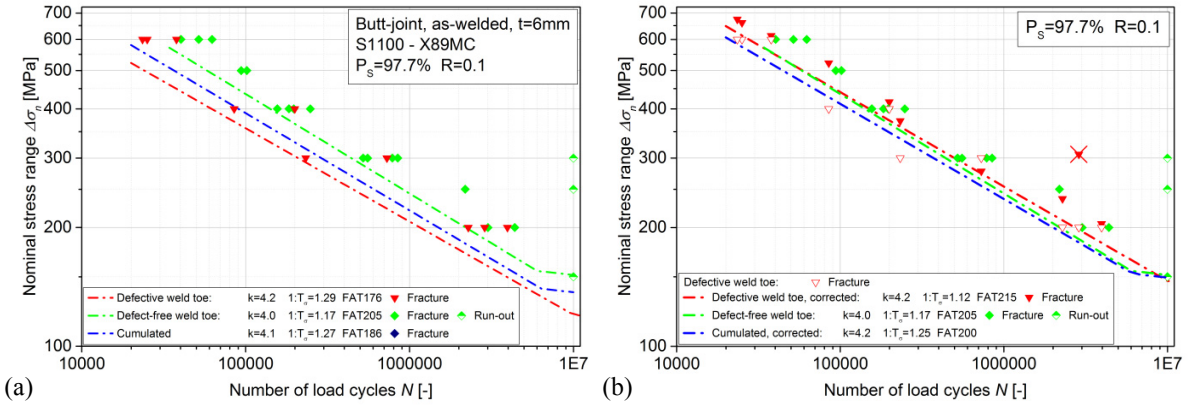

Fig. 7. (a) Fatigue test results for defect-free and defective specimen; (b) SN-curve containing the corrected results of defective specimen

5. Conclusions

This work compares the fatigue strength of defect-free-welded and undercut-defective ultra high-strength steel butt joints. The examined macroscopic undercuts are detectable by visual inspection. All defective specimens are spatial optically measured in order to determine the local weld topography prior to fatigue testing. On the basis of these geometrical measurements, a digital image process based evaluation method is set-up to identify the local undercut depth and the weld reinforcement angle. The fatigue tests show a distinct decrease of fatigue strength in the presence of weld defects. Although, especially in high-cycle fatigue region, the absolute value of the difference is much smaller than expected due to effects of local residual stress state. But the overall fatigue strength of the examined undercut-imperfected butt joints can be traced back to very small geometric defects at the weld toe having similar impact on the cyclic behavior. The main focus of the fatigue assessment in this work is the link of the fatigue test results of the undercut-defective and non-defective specimen in order to ensure comparability. This is done by the use of a local support effect concept with cyclic test data of S1100 base material. Every defective specimen's geometry undergoes a linear-elastic finite element simulation to determine the stress concentration and the local relative stress gradient at the respective crack initiation point. A recalculation of the fatigue strength of the defective specimen on the basis of local support effect is performed. The result of this procedures shows, that the undercut-defective specimens are within the scatter band of the non-defective if support effects are considered. Summing up, by the aid of this methodology the effect of arbitrarily shaped defects, such as undercuts, can be assessed regarding to fatigue strength.

Acknowledgements

Special thanks are given to the Austrian Research Promotion Agency (FFG), who founded the research project by funds of the Federal Ministry for Transport, Innovation and Technology (bmvit) and the Federal Ministry of Economics and Labour (BMWA), and to all the industry partners for the supply of material and the fabrication work done.

References

[1] Hobbacher, A.: The new IIW recommendations for fatigue assessment of welded joints and components – A comprehensive code recently updated; *International Journal of Fatigue* 31 (2009) 1, pp. 50–58.

[2] Forschungskuratorium Maschinenbau: Rechnerischer Festigkeitsnachweis für Maschinenbauteile aus Stahl, Eisenguss- und Aluminiumwerkstoffen, 2012.

[3] Laitinen, R.; Valkonen, I.; Kömi, J.: Influence of the base Material Strength and Edge Preparation on the Fatigue Strength of the Structures Made by High and Ultra-high Strength Steels; *Procedia Engineering* 66 (2013), pp. 282–291.
[4] Leitner, M.; Stoschka, M.; Eichlseder, W.: Fatigue enhancement of thin-walled, high-strength steel joints by high-frequency mechanical impact treatment; *Welding in the World* 58 (2014) 1, pp. 29–39.
[5] Stoschka, M.; Leitner, M.; Posch, G.; Eichlseder, W.: Effect of high-strength filler metals on the fatigue behaviour of butt joints; *Welding in the World* 57 (2013) 1, pp. 85–96.
[6] Yildirim, H. C.: Review of fatigue data for welds improved by tungsten inert gas dressing; *International Journal of Fatigue* 79 (2015), pp. 36–45.
[7] Berg, J.; Stranghöner, N.: Fatigue Strength of Welded Ultra High Strength Steels Improved by High Frequency Hammer Peening; *Procedia Materials Science* 3 (2014), pp. 71–76.
[8] Barsoum, Z.: Fatigue Design of Welded Structures — Some Aspects of Weld Quality and Residual Stresses; *Welding in the World* 55 (2011) 11-12, pp. 2–11.
[9] Nykänen, T.; Marquis, G.; Björk, T.: Effect of weld geometry on the fatigue strength of fillet welded cruciform joints; in *Proceedings of the International Symposium on Integrated Design and Manufacturing of Welded Structures* (Marquis, G. Ed.), Lappeenranta University of Technology, Lappeenranta, 2007.
[10] Baumgartner, J.; Bruder, T.: Influence of weld geometry and residual stresses on the fatigue strength of longitudinal stiffeners; *Welding in the World* 57 (2013) 6, pp. 841–855.
[11] Cerit, M.; Kokumer, O.; Genel, K.: Stress concentration effects of undercut defect and reinforcement metal in butt welded joint; *Engineering Failure Analysis* 17 (2010) 2, pp. 571–578.
[12] Nguyen, N. T.; Wahab, M. A.: The effect of undercut, misalignment and residual stresses on the fatigue behaviour of butt welded joints; *Fatigue & Fracture of Engineering Materials and Structures* 19 (1996) 6, pp. 769–778.
[13] Alicona GmbH: InfiniteFocus technical specification, 2014.
[14] Hough, P. V. C.: Method and means for recognizing complex patterns, 1962.
[15] ASTM E739: Practice for Statistical Analysis of Linear or Linearized Stress-Life (S-N) and Strain-Life (e-N) Fatigue Data, 2010.
[16] Dengel, D.; Harig, H.: Estimation of the fatigue limit by progressively ‐ increasing load tests; *Fatigue & Fracture of Engineering Materials and Structures* 3 (1980) 2, pp. 113–128.
[17] Sonsino, C. M.: Course of SN-curves especially in the high-cycle fatigue regime with regard to component design and safety; *International Journal of Fatigue* 29 (2007) 12, pp. 2246–2258.
[18] Ottersböck, M. J.; Leitner, M.; Stoschka, M.; Maurer, W.: Fatigue strength of welded ultra high-strength steel joints; in *Proceedings of the IIW International Conference 2015* (International Institute of Welding Ed.), 2015.
[19] Eichlseder, W.: Fatigue analysis by local stress concept based on finite element results; *Computers & Structures* 80 (2002) 27-30, pp. 2109–2113.